

Thermal Properties and Crystal Structure of BaC₄H₄O₆ Single Crystals

Takanori Fukami¹, Seiya Hiyajyo¹, Shuta Tahara¹, Chitoshi Yasuda¹

¹Department of Physics and Earth Sciences, Faculty of Science, University of the Ryukyus, Japan

Correspondence: Takanori Fukami, Department of Physics and Earth Sciences, Faculty of Science, University of the Ryukyus, Okinawa 903-0213, Japan. E-mail: fukami@sci.u-ryukyu.ac.jp

Received: November 2, 2016 Accepted: November 30, 2016 Online Published: December 2, 2016

doi:10.5539/ijc.v9n1p30

URL: <http://dx.doi.org/10.5539/ijc.v9n1p30>

Abstract

Single crystals of barium L-tartrate, BaC₄H₄O₆, were grown at 308 K by a gel method using silica gel as the growth medium. Differential scanning calorimetry, thermogravimetric-differential thermal analysis, and X-ray diffraction measurements were performed on the single crystals. The space group symmetry (orthorhombic, *P*2₁2₁2₁) and structural parameters were determined at room temperature. The crystal structure consisted of BaO₉ polyhedra, C₄H₄O₆ molecules, and zig-zag hydrogen-bonded chains along the *a*- and *c*-axes linked by O–H···O and C–H···O hydrogen bonds between adjacent molecules. Weight losses due to thermal decomposition of BaC₄H₄O₆ occurred in the temperature range of 450–1530 K. We suggest that the evolution of 2H₂, 2CO, CO, (1/2)O₂, and O₂ gases caused the observed weight losses and that the decomposition product, barium monocarbide BaC, formed a residue in the vessel.

Keywords: BaC₄H₄O₆, BaC, thermal decomposition, TG-DTA, X-ray diffraction

1. Introduction

Tartaric acid (chemical formula: C₄H₆O₆; systematic name: 2,3-dihydroxybutanedioic acid) is found in grapes, currants, gooseberries, oranges, apples, and in most acidulous fruits. It has two chiral carbon atoms in its structure, which provides for four possible different forms of chiral, racemic, and achiral isomers: L(+)-tartaric, D(–)-tartaric, racemic (DL-) tartaric, and meso-tartaric acid (Bootsma & Schoone, 1967; Fukami, Tahara, Yasuda, & Nakasone, 2016b; Song, Teng, Dong, Ma, & Sun, 2006). The most common form in nature is L-tartaric acid, while meso-tartaric acid is man-made and does not occur in nature. Solutions of L- and D-tartaric acid rotate the plane of polarized light to the left and right, respectively, whereas of DL- and meso-tartaric acid do not induce rotation of plane-polarized light. The properties of optically active molecules derived from tartaric acid were discovered by Biot (Lowry, 1923).

Many tartrate compounds are formed by the reaction of tartaric acid with compounds containing positive ions (two monovalent cations or one divalent cation) (Boese & Heinemann, 1993; Buschmann & Luger, 1985; Fukami, Hiyajyo, Tahara, & Yasuda, 2016a; Fukami et al., 2016c; Hawthorne, Borys, & Ferguson, 1982; Labutina, Marychev, Portnov, Somov, & Chuprunov, 2011; Silgo, Platas, Pérez, López, & Torres, 1999; Weil, 2015). These compounds are used in numerous industrial applications, for example, as transducers and in linear and non-linear mechanical devices because of their excellent dielectric, ferroelectric, piezoelectric, and nonlinear optical properties (Firdous et al., 2010; Kader et al., 1991; Torres et al., 2002). Several types of tartaric acid crystals, such as potassium hydrogen tartrate (KHC₄H₄O₆), and calcium tartrate (CaC₄H₄O₆), develop naturally in bottled wine and are the major component of the harmless sediment found in wine (Boese & Heinemann, 1993; Buschmann & Luger, 1985; Derewenda, 2008; Hawthorne et al., 1982). The crystalline tartrate sediment as a by-product has to be removed from the wine after yeast fermentation of the grape juice. More than 150 years ago, Louis Pasteur first separated the two enantiomers of sodium ammonium tartrate (NaNH₄C₄H₄O₆) by utilizing the asymmetric habit of their crystals (Gal, 2013; Pasteur, 1848). In addition, he discovered the change in optical rotation induced by the different structures of each enantiomer in water solution. The discovery of enantiomers has played an important role in advancing the scientific understanding of molecular chirality.

Silgo et al. (1999) established the crystal structure of barium L-tartrate BaC₄H₄O₆ by means of single-crystal X-ray diffraction at room temperature. The crystal structure was orthorhombic with space group *P*2₁2₁2₁, and consisted of BaO₉ polyhedra, C₄H₄O₆ molecules, and O–H···O hydrogen bonds. The positions of hydrogen atoms were calculated based on geometric criteria (O–H and C–H distances of 0.82 and 0.98 Å, respectively), and the atoms were included in the refinement at the fixed positions with constant isotropic thermal parameters. Shah and Patel (2010) reported the stretching modes of O–H, C–H, C–O, C–C, and Ba–O in BaC₄H₄O₆ based on FTIR and X-ray diffraction measurements. Moreover, they confirmed that the crystal structure was essentially the same as that reported by Silgo et al (1999).

The purpose of this study is to determine the exact crystal structure of $\text{BaC}_4\text{H}_4\text{O}_6$, including the positions of all hydrogen atoms, at room temperature using X-ray diffraction measurements. We report the thermal properties of this compound, as determined by means of differential scanning calorimetry (DSC) and thermogravimetric-differential thermal analysis (TG-DTA).

2. Experimental

2.1 Crystal Growth

Light yellow block crystals of $\text{BaC}_4\text{H}_4\text{O}_6$ were grown in silica gel medium at 308 K using the single test tube diffusion method. The gel was prepared in the test tube (length of 200 mm and diameter of 30 mm) using aqueous solutions of Na_2SiO_3 (33.7 g of 10.9 wt%), L-tartaric acid $\text{C}_4\text{H}_6\text{O}_6$ (28.8 g of 13.0 wt%), and CH_3COOH (24.6 g of 10.7 wt%) and aged for several days. A solution of $\text{Ba}(\text{NO}_3)_2$ (23.7 g of 15.5 wt%) was heated to boiling point until complete dissolution of $\text{Ba}(\text{NO}_3)_2$ and, after cooling to room temperature, was gently poured on top of the gel. The crystals were harvested after five months. Samples used for measurements were cut from transparent areas on the tips of crystal.

2.2 X-ray Crystal Structure Determination

The X-ray diffraction measurements were carried out using a Rigaku Saturn CCD X-ray diffractometer with graphite-monochromated $\text{Mo } K_\alpha$ radiation ($\lambda = 0.71073 \text{ \AA}$). The diffraction data were collected at 298 K using an ω scan mode with a crystal-to-detector distance of 40 mm, and processed using the CrystalClear software package. The intensity data were corrected for Lorentz polarization and absorption effects. The structure was solved by direct methods using the SIR2011 program and refined on F^2 by full-matrix least-squares methods using the SHELXL-2013 program in the WinGX package (Burla et al., 2012; Farrugia, 2012; Sheldrick, 2015).

Table 1. Crystal data, intensity collection, and structure refinement for $\text{BaC}_4\text{H}_4\text{O}_6$

Compound, M_r	$\text{BaO}_6\text{C}_4\text{H}_4$, 285.41
Crystal color	Colorless
Measurement temperature	298 K
Crystal system, space group	Orthorhombic, $P2_12_12_1$
Lattice constants	$a = 8.3986(2) \text{ \AA}$, $b = 9.0370(3) \text{ \AA}$, $c = 8.1924(3) \text{ \AA}$
V , Z	$621.79(3) \text{ \AA}^3$, 4
$D(\text{cal.})$, $\mu(\text{Mo } K_\alpha)$, $F(000)$	3.049 Mg m^{-3} , 6.365 mm^{-1} , 528
Sample shape, size in diameter	Sphere, $2r = 0.30 \text{ mm}$
θ range for data collection	$3.31\text{--}37.87^\circ$
Index ranges	$-14 \leq h \leq 14$, $-15 \leq k \leq 15$, $-13 \leq l \leq 13$
Reflections collected, unique	17681, 3258 [$R(\text{int}) = 0.0306$]
Completeness to θ_{max}	97.9 %
Absorption correction type	Spherical
Transmission factor $T_{\text{min}}\text{--}T_{\text{max}}$	0.2428–0.2746
Date [$I > 2\sigma(I)$], parameter	3110, 117
Final R indices	$R_1 = 0.0190$, $wR_2 = 0.0360$
R indices (all data)	$R_1 = 0.0224$, $wR_2 = 0.0376$
Weighting scheme	$w = 1/[\sigma^2(F_o^2) + (0.0174P)^2 + 0.1072P]$, $P = (F_o^2 + 2F_c^2)/3$
Goodness-of-fit on F^2	1.057
Flack parameter	-0.032(7)
Extinction coefficient	0.0141(5)
Largest diff. peak and hole	1.721 and -1.198 e\AA^{-3}

2.3 Thermal Measurements

DSC and TG-DTA measurements were respectively carried out in the temperature ranges of 102–370 K and 300–1530 K, using DSC7020 and TG-DTA7300 systems from Seiko Instruments Inc. Aluminium (for DSC) and platinum (for TG-DTA) open pans without a cover were used as the measuring vessel and reference pan. Fine powder samples prepared by grinding the some cutting crystals of colorless were used for the measurements. The sample amount varied between 4.60 and 4.98 mg, and the heating rates were either 5 or 10 K min^{-1} under the flow of nitrogen gas.

3. Results and Discussion

3.1 Crystal Structure

The crystal structure of $\text{BaC}_4\text{H}_4\text{O}_6$ was determined by the single-crystal X-ray diffraction at room temperature. The lattice parameters calculated from all observed reflections showed that the crystal belongs to orthorhombic system. The intensity statistics and systematic extinctions of the observed reflections strongly revealed that the crystal structure is an acentric space group of $P2_12_12_1$. Thus, the space group of $\text{BaC}_4\text{H}_4\text{O}_6$ was determined to be orthorhombic $P2_12_12_1$ with cell parameters $a = 8.3986(2)$ Å, $b = 9.0370(3)$ Å, and $c = 8.1924(3)$ Å. The atomic coordinates and thermal parameters for $\text{BaC}_4\text{H}_4\text{O}_6$, including the positions of all hydrogen atoms, were refined at room temperature. A final R -factor of 1.90% was calculated for 3110 unique observed reflections. The relevant crystal data, and a summary of the intensity data collection and structure refinement parameters are given in Table 1. Figure 1 shows a projected view of the $\text{BaC}_4\text{H}_4\text{O}_6$ crystal structure in the bc -plane. The positional parameters in fractions of the unit cell, and the thermal parameters are listed in Table 2. Selected bond lengths (in Å) and angles (in degrees) are given in Table 3. The hydrogen-bond geometry (in Å and degrees) is presented in Table 4.

Table 2. Atomic coordinates and thermal parameters ($\times 10^4$ Å²) with standard deviations in brackets. The anisotropic thermal parameters are defined as $\exp[-2\pi^2(U_{11}a^{*2}h^2 + U_{22}b^{*2}k^2 + U_{33}c^{*2}l^2 + 2U_{23}b^*c^*kl + 2U_{13}a^*c^*hl + 2U_{12}a^*b^*hk)]$. The isotropic thermal parameters (Å²) for H atoms are listed under U_{11} .

Atom	x	y	z	U_{11}	U_{22}	U_{33}	U_{23}	U_{13}	U_{12}
Ba	0.27986(2)	0.76534(2)	0.40953(2)	122.8(6)	144.8(5)	129.2(5)	-2.2(4)	7.2(5)	-10.8(4)
O(1)	0.2408(2)	0.0703(2)	0.3543(2)	150(9)	205(8)	184(8)	-1(6)	-15(7)	-28(6)
O(2)	0.4188(2)	0.1569(2)	0.1757(2)	185(9)	284(10)	120(8)	32(7)	-12(7)	-26(8)
O(3)	0.6070(2)	0.2646(2)	0.4085(2)	161(7)	206(7)	149(7)	-13(9)	10(6)	-72(6)
O(4)	0.5586(2)	-0.0593(2)	0.4695(2)	173(9)	138(7)	131(8)	-10(6)	20(7)	8(6)
O(5)	0.7266(3)	0.0118(2)	0.7356(3)	268(10)	295(10)	288(11)	-93(8)	-160(10)	111(10)
O(6)	0.5465(3)	0.1783(3)	0.8193(2)	221(9)	262(10)	150(8)	-61(7)	-3(7)	-8(8)
C(1)	0.3674(3)	0.1385(3)	0.3169(3)	121(10)	140(9)	133(10)	5(7)	-28(8)	14(7)
C(2)	0.4655(3)	0.1949(3)	0.4631(3)	131(10)	139(9)	125(9)	-6(8)	0(7)	-1(7)
C(3)	0.4995(3)	0.0579(3)	0.5683(3)	134(9)	140(9)	94(10)	-7(7)	-4(7)	-3(7)
C(4)	0.6010(3)	0.0859(3)	0.7193(3)	163(10)	170(10)	114(9)	6(8)	-18(8)	-19(8)
H(1)	0.635(5)	0.328(5)	0.490(5)	0.030(11)					
H(2)	0.602(5)	-0.041(5)	0.398(5)	0.024(10)					
H(3)	0.408(4)	0.257(4)	0.515(4)	0.015(8)					
H(4)	0.397(5)	0.029(4)	0.617(4)	0.020(9)					

The obtained crystal structure of $\text{BaC}_4\text{H}_4\text{O}_6$ is very similar to that previously reported by Silgo et al. (1999), and very different from those of the $\text{CaC}_4\text{H}_4\text{O}_6 \cdot 4\text{H}_2\text{O}$ and $\text{SrC}_4\text{H}_4\text{O}_6 \cdot 4\text{H}_2\text{O}$ crystals because it does not contain any water molecules (Boese & Heinemann, 1993; Fukami et al., 2016c; Hawthorne et al., 1982). The fundamental features of the obtained structure are as follows. Each Ba atom in the unit cell is surrounded by nine O atoms at distances from 2.771(2) to 2.884(2) Å, forming a BaO_9 polyhedron, as listed in Table 3. The average Ba–O distance is 2.818 Å. The volume of the BaO_9 polyhedron (at the distance of 2.818 Å) is larger than those of the CaO_8 and SrO_8 dodecahedra (at average Ca–O and Sr–O distances of 2.455 and 2.594 Å, respectively) in the calcium and strontium salts (Boese & Heinemann, 1993; Fukami et al., 2016c; Hawthorne et al., 1982). This is probably because of the difference in ionic radius between Ba^{2+} and Ca^{2+} (or Sr^{2+}) ions. Moreover, the presence or absence of internal water molecules in the structure may be related to the difference in volume between the BaO_9 polyhedron and the CaO_8 (or SrO_8) dodecahedron. The lengths of six O–C bonds in the $\text{C}_4\text{H}_4\text{O}_6$ molecule are in the range of 1.256(3)–1.422(3) Å, as listed in Table 3. The variation in O–C distances is probably related to differences in bond type. The lengths of single and double O–C bonds in organic molecules are around 1.43 and 1.22 Å, respectively. The O(3)–C(2) and O(4)–C(3) bond lengths (hydroxyl group) are about 1.42 Å. Thus, these two O–C bonds have single-bond character. Because the lengths of the remaining four O–C bonds are about 1.26 Å, these bonds have double-bond character. Additionally, the lengths of three C–C bonds are in the range of 1.523(3)–1.540(3) Å, similar to that (around 1.54 Å) of single C–C bonds in organic molecules, indicating these bonds have single-bond character. Thus, the characteristic features of the $\text{C}_4\text{H}_4\text{O}_6$ molecule in the $\text{BaC}_4\text{H}_4\text{O}_6$ crystal are very similar to that in the $\text{SrC}_4\text{H}_4\text{O}_6 \cdot 4\text{H}_2\text{O}$ crystal (Fukami et al., 2016c).

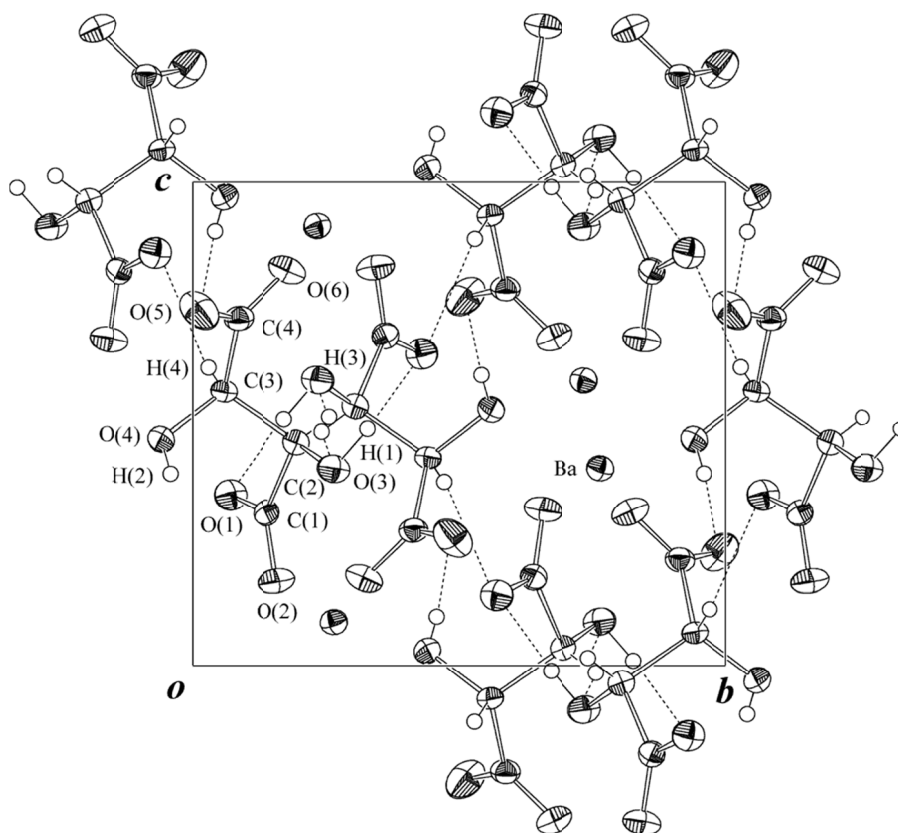


Figure 1. ORTEP projection in the bc -plane of $\text{BaC}_4\text{H}_4\text{O}_6$ structure with 70% probability-displacement thermal ellipsoids

The solid and short dashed lines show the $\text{O}-\text{H}\cdots\text{O}$ and $\text{C}-\text{H}\cdots\text{O}$ hydrogen bonds in Table 4.

Table 3. Selected interatomic distances (in Å) and angles (in degrees)

$\text{Ba}-\text{O}(1)^{(a)}$	2.812(2)	$\text{Ba}-\text{O}(2)^{(b)}$	2.802(2)
$\text{Ba}-\text{O}(2)^{(c)}$	2.834(2)	$\text{Ba}-\text{O}(3)^{(b)}$	2.773(2)
$\text{Ba}-\text{O}(4)^{(d)}$	2.811(2)	$\text{Ba}-\text{O}(4)^{(a)}$	2.870(2)
$\text{Ba}-\text{O}(5)^{(d)}$	2.808(2)	$\text{Ba}-\text{O}(6)^{(e)}$	2.771(2)
$\text{Ba}-\text{O}(6)^{(f)}$	2.884(2)	$\text{O}(1)-\text{C}(1)$	1.267(3)
$\text{O}(2)-\text{C}(1)$	1.245(3)	$\text{O}(3)-\text{C}(2)$	1.418(3)
$\text{O}(4)-\text{C}(3)$	1.422(3)	$\text{O}(5)-\text{C}(4)$	1.256(3)
$\text{O}(6)-\text{C}(4)$	1.256(3)	$\text{C}(1)-\text{C}(2)$	1.540(3)
$\text{C}(2)-\text{C}(3)$	1.536(3)	$\text{C}(3)-\text{C}(4)$	1.523(3)
$\text{O}(1)-\text{C}(1)-\text{O}(2)$	125.5(2)	$\text{O}(1)-\text{C}(1)-\text{C}(2)$	114.9(2)
$\text{O}(2)-\text{C}(1)-\text{C}(2)$	119.5(2)	$\text{O}(3)-\text{C}(2)-\text{C}(1)$	110.5(2)
$\text{O}(3)-\text{C}(2)-\text{C}(3)$	112.3(2)	$\text{O}(4)-\text{C}(3)-\text{C}(2)$	110.3(2)
$\text{O}(4)-\text{C}(3)-\text{C}(4)$	113.0(2)	$\text{O}(5)-\text{C}(4)-\text{O}(6)$	126.2(3)
$\text{O}(5)-\text{C}(4)-\text{C}(3)$	117.8(2)	$\text{O}(6)-\text{C}(4)-\text{C}(3)$	115.9(2)
$\text{C}(3)-\text{C}(2)-\text{C}(1)$	105.6(2)	$\text{C}(4)-\text{C}(3)-\text{C}(2)$	115.2(2)

Symmetry codes: (a) $x, y+1, z$; (b) $-x+1, y+1/2, -z+1/2$; (c) $-x+1/2, -y+1, z+1/2$; (d) $x-1/2, -y+1/2, -z+1$; (e) $-x+1, y+1/2, -z+3/2$; (f) $-x+1/2, -y+1, z-1/2$.

The observed crystal structure contains $\text{O}-\text{H}\cdots\text{O}$ and $\text{C}-\text{H}\cdots\text{O}$ hydrogen bonds formed between adjacent $\text{C}_4\text{H}_4\text{O}_6$ molecules, as shown in Fig. 1 and Table 4. The lengths of the hydrogen bonds are in the range of 2.667(3)–3.303(3) Å, where the $\text{C}-\text{H}\cdots\text{O}$ bonds are much longer than the $\text{O}-\text{H}\cdots\text{O}$ bonds. Thus, the bond strength of the $\text{C}-\text{H}\cdots\text{O}$ bonds is significantly lower than that of the $\text{O}-\text{H}\cdots\text{O}$ bonds. The structure based on the presence of the $\text{C}-\text{H}\cdots\text{O}$ hydrogen bonds is substantially different from that in the $\text{SrC}_4\text{H}_4\text{O}_6 \cdot 4\text{H}_2\text{O}$ crystal, which does not form a similar hydrogen bond network

(Fukami et al., 2016c). As shown in Fig. 1, there are zig-zag hydrogen-bonded chains along the *c*-axis, which consist of O(4)–H(2)⋯O(5) and C(3)–H(4)⋯O(1) bonds between adjacent C₄H₄O₆ molecules. Moreover, there are zig-zag hydrogen-bonded chains along the *a*-axis, which consist of O(3)–H(1)⋯O(1) and C(2)–H(3)⋯O(3) bonds between molecules.

The calculated angle between the two least-squares planes of atoms, O(1)O(2)O(3)C(1)C(2) and O(4)O(5)O(6)C(3)C(4), in the C₄H₄O₆ molecule is 67.17(8)°. The angles in the strontium tartaric acid, monohydrate racemic (MDL-) tartaric acid, L- tartaric acid, and D-tartaric acid crystals are 88.7(1)°, 72.79(4)°, 56.33(5)°, and 56.34(5)°, respectively (Fukami et al., 2016b, 2016c). Thus, the torsional strain in the C₄H₄O₆ unit of BaC₄H₄O₆ is smaller than that in the strontium salt and most similar to that in the MDL-tartaric acid crystal.

Table 4. Hydrogen bond distances (in Å) and angles (in degrees)

D–H⋯A	D–H	H⋯A	D⋯A	<D–H⋯A
O(3)–H(1)⋯O(1) ^(a)	0.91(4)	1.81(4)	2.696(3)	165(4)
O(4)–H(2)⋯O(5) ^(b)	0.71(4)	1.98(4)	2.667(3)	164(5)
C(2)–H(3)⋯O(3) ^(c)	0.85(4)	2.61(4)	3.210(3)	128(3)
C(3)–H(4)⋯O(1) ^(d)	0.98(4)	2.44(4)	3.303(3)	147(3)

Symmetry codes: (a) $x+1/2, -y+1/2, -z+1$; (b) $-x+3/2, -y, z-1/2$; (c) $x-1/2, -y+1/2, -z+1$; (d) $-x+1/2, -y, z+1/2$.

3.2 Thermal Analyses

DSC measurements on the powder sample of BaC₄H₄O₆ were performed in the temperature range from 102 to 370 K at a heating rate of 5 K min⁻¹. No endothermic or exothermic peak in the DSC curve was observed in the temperature range. In general, it is accepted that a clear peak in DSC curve is attributed to a change in exchange energy at a phase transition. Thus, the obtained result indicates that there is no phase transition in the temperature range of 102–370 K for the BaC₄H₄O₆ crystal.

Figure 2 shows the TG, differential TG (DTG), and DTA curves of BaC₄H₄O₆ in the temperature range of 300–1530 K. The sample weight (powder) used for the measurements was 4.98 mg, and the heating rate was 10 K min⁻¹ under a nitrogen gas flow of 300 ml min⁻¹. The DTA curve shows eleven apparent small endothermic peaks, and the DTG curve has nine peaks, including some small peaks. The temperatures describing the DTA and DTG peaks are shown in Table 5 and indicated by arrows in Fig. 2. At temperatures below 1400 K, the DTG peaks correspond to the respective DTA peaks, except for very small peaks. The DTG curve, which is the first derivative of the TG curve, reveals the temperature dependence of the rate of weight loss. Thus, the DTA peaks are associated with maximum rates of weight loss in the TG curve due to thermal decomposition of the sample.

Table 5. Peak temperatures (K) obtained from DTA and DTG curves of BaC₄H₄O₆

DTA	537	647	733	999	1051	1078	1272	1323	1441	1456	1496
DTG	538	601	647	728	1002	1018	1272	1309	1322		

Table 6. TG results of thermal decomposition of BaC₄H₄O₆

Temp. range [K]	Weight loss (obs.) [%]	Weight loss (cal.) [%]	Eliminated molecules
450–545	1.9	1.4	2H ₂
545–655	16.6	19.6	2CO
655–840	9.7	9.8	CO
840–1060	7.5	5.6	(1/2)O ₂
1060–1530	12.3	11.2	O ₂
Total	47.9	47.7	

The TG curve shows the temperature dependence of the weight loss of the BaC₄H₄O₆ crystal. The weight loss around 537 K in the TG curve was determined to be 1.9% in the temperature range from 450 to 545 K. We assume that the weight loss is caused by the elimination of two moles of H₂ gas. The theoretical weight loss is calculated to be 1.4% [=4×1.01/285.41], and is very close to the experimental weight loss of 1.9% at around 537 K. The weight losses around 647 and 733 K were determined to be 16.6% and 9.7% in the temperature ranges of 545–655 K and 655–840 K, respectively. We assume that the weight losses are caused by the elimination of CO gas (two moles and one mole). The theoretical weight losses are calculated to be 19.6% [=2×(12.01+16.00)/285.41] and 9.8% [= (12.01+16.00)/285.41] and again, are close to the experimental weight losses of 16.6% and 9.7% at around 647 and 733 K, respectively. The different evaporation temperatures of CO gas likely result from the different routes of CO generation, from the hydroxyl (H–C–O–H) or carbonyl (O–C=O) groups of the C₄H₄O₆ molecule. The weight losses around 999 and 1051 K were

determined to be 7.5% and 12.3% in the temperature ranges of 840–1060 K and 1060–1530 K, respectively. We assume that the weight losses are caused by the evolution of O₂ gas (half mole and one mole). The theoretical weight losses are calculated to be 5.6% [=16.00/285.41] and 11.2% [=2×16.00/285.41], and are close to the experimental weight losses of 7.5% and 12.3% at around 999 and 1051 K, respectively. It is implied that the half mole of O₂ gas is generated from one O atom in the carbonyl group remained by the evolution of 3CO gases in the temperature range of 545–840 K mentioned above. Table 6 summarizes the experimental and theoretical weight losses in each temperature range.

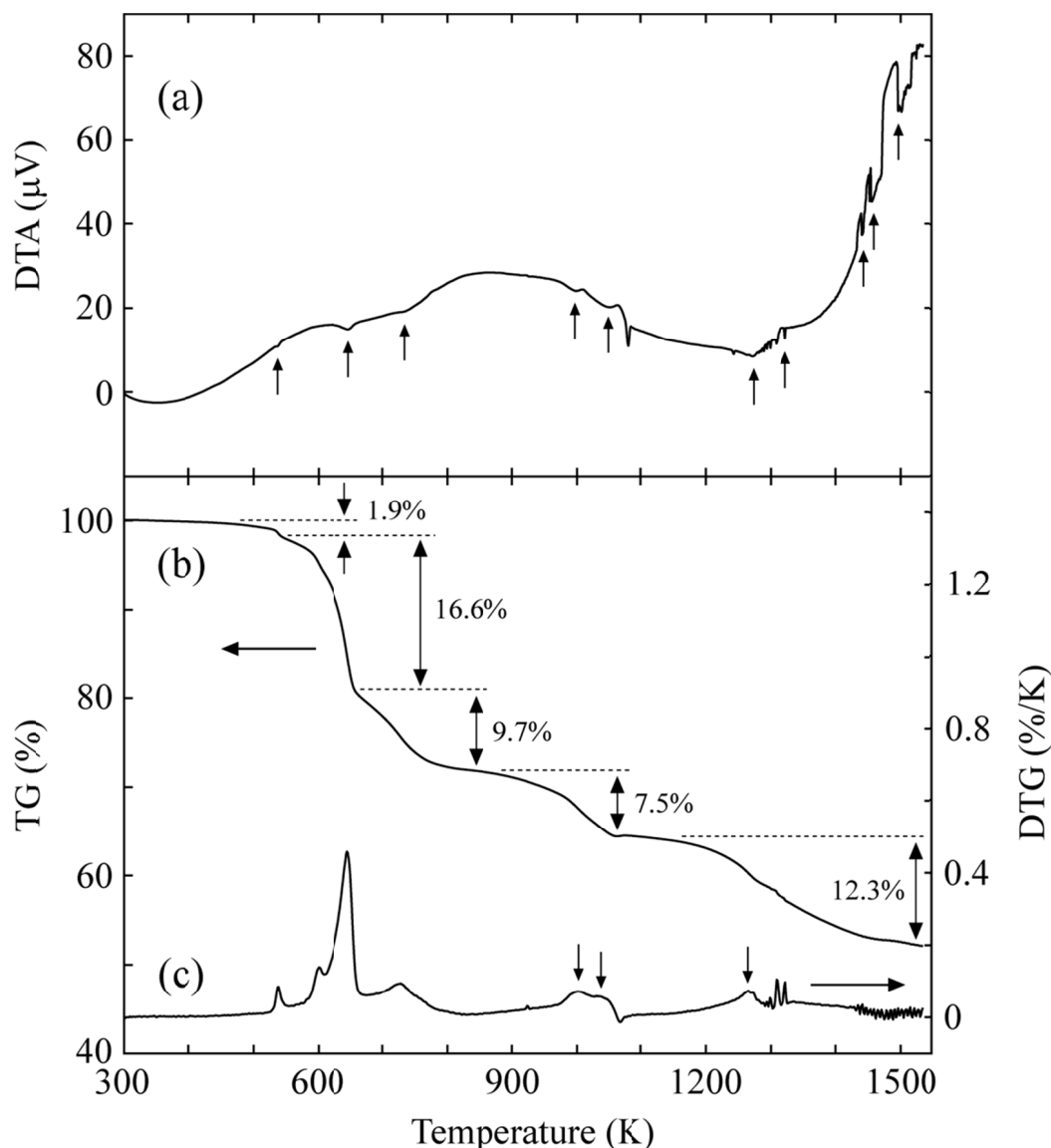
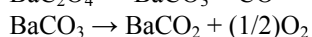
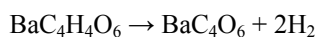
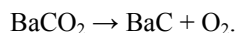


Figure 2. (a) DTA, (b) TG, and (c) DTG curves of BaC₄H₄O₆ crystal on heating. The positions of small peaks are indicated by arrows

Sample weight (powder) was 4.98 mg, and the heating rate was 10 K min⁻¹ under N₂ gas flow of 300 ml min⁻¹.

The total theoretical weight loss from BaC₄H₄O₆ is 47.7%. This value is very close to the total experimental weight loss of 47.9%. Thus, the slight differences between the experimental and theoretical weight loss values at each temperature range in Table 6 are probably due to the overlapping of the temperature ranges corresponding to the decomposition reactions. Summarizing the considerations mentioned above, the chemical reactions involved in the thermal decomposition of BaC₄H₄O₆ can be described by the following chemical equations:





After all gases had evolved, barium monocarbide (BaC) remains in the vessel, as suggested by the chemical equations listed above. In fact after the measurements (heated up to 1530 K), the inside surface of the open vessel was found to be turned black in color. The black substance is considered to be barium monocarbide. Similarly, a chalky white substance was confirmed to remain in the vessel after the $\text{SrC}_4\text{H}_4\text{O}_6 \cdot 4\text{H}_2\text{O}$ crystal was heated up to 1250 K, and was suggested to be strontium oxide SrO (Fukami et al., 2016c). The electron configurations for Ba and Sr atoms are $[\text{Kr}] 5s^2 5p^6 6s^2$ and $[\text{Kr}] 5s^2$, respectively. Thus, both the atoms convert into a divalent positive ion when two electrons are removed from the outermost shell. Moreover, the valence electron configuration $[\text{Kr}] 5s^2 5p^3 6s^1$ for barium is a stable electron structure, and the Ba atom can convert into a tetravalent positive ion. This is also deduced from the presence of BaO_2 produced by the reaction of BaO and $(1/2)\text{O}_2$. It is concluded that tetravalent Ba^{4+} ion is necessary to produce BaC at high temperatures. The observed process during the thermal decomposition and the remaining substance in the vessel are very different from those in the case of the $\text{SrC}_4\text{H}_4\text{O}_6 \cdot 4\text{H}_2\text{O}$ crystal (Fukami et al., 2016c).

4. Conclusion

Single crystals of barium L-tartrate, $\text{BaC}_4\text{H}_4\text{O}_6$, were grown in silica gel medium at 308 K by the diffusion method. The thermal properties and crystal structure of the single crystals are studied by DSC, TG-DTA, and X-ray diffraction. The room temperature crystal structure, including the positions of the hydrogen atoms, is determined to be orthorhombic with space group $P2_12_12_1$ by means of single-crystal X-ray diffraction. It is confirmed that the structure consists of BaO_9 polyhedra, $\text{C}_4\text{H}_4\text{O}_6$ molecules, and zig-zag hydrogen-bonded chains along the *a*- and *c*-axes linked by $\text{O}-\text{H}\cdots\text{O}$ and $\text{C}-\text{H}\cdots\text{O}$ hydrogen bonds between adjacent $\text{C}_4\text{H}_4\text{O}_6$ molecules. No phase transition is observed in the temperature range of 102–450 K. Weight losses during the thermal decomposition of $\text{BaC}_4\text{H}_4\text{O}_6$ occurs in the temperature range of 450–1530 K. The chemical equations illustrating the decomposition reactions of $\text{BaC}_4\text{H}_4\text{O}_6$ are presented with the corresponding temperature ranges. It is suggested that the weight losses are caused by the evolution of 2H_2 , 2CO , CO , $(1/2)\text{O}_2$, and O_2 gases, and that the residual black substance in the vessel after decomposition is barium monocarbide (BaC), which comprises tetravalent barium (Ba^{4+}) ion.

References

- Boese, R., & Heinemann, O. (1993). Crystal structure of calcium tartrate tetrahydrate, $\text{C}_4\text{H}_4\text{O}_6\text{Ca}(\text{H}_2\text{O})_4$. *Z. Kristallogr.*, 205(1–2), 348–349. <http://dx.doi.org/10.1524/zkri.1993.205.12.348>
- Bootsma, G. A., & Schoone, J. C. (1967). Crystal structures of mesotartaric acid. *Acta Crystallogr.*, 22(4), 522–532. <http://dx.doi.org/10.1107/S0365110X67001070>
- Burla, M. C., Caliandro, R., Camalli, M., Carrozzini, B., Cascarano, G. L., Giacovazzo, C., ... & Spagna, R. (2012). SIR2011: a new package for crystal structure determination and refinement. *J. Appl. Crystallogr.*, 45(2), 357–361. <http://dx.doi.org/10.1107/S0021889812001124>
- Buschmann, J., & Luger, P. (1985). Structure of potassium hydrogen (+)-tartrate at 100 K, $\text{K}^+\cdot\text{C}_4\text{H}_5\text{O}_6^-$. *Acta Crystallogr.*, C41(2), 206–208. <http://dx.doi.org/10.1107/S0108270185003341>
- Derewenda, Z. S. (2008). On wine, chirality and crystallography. *Acta Crystallogr.*, A64(1), 246–258. <http://dx.doi.org/10.1107/S0108767307054293>
- Farrugia, L. J. (2012). WinGX and ORTEP for Windows: an update. *J. Appl. Crystallogr.*, 45(4), 849–854. <http://dx.doi.org/10.1107/S0021889812029111>
- Firdous, A., Quasim, I., Ahmad, M. M., & Kotru, P. N. (2010). Dielectric and thermal studies on gel grown strontium tartrate pentahydrate crystals. *Mull. Mater. Sci.*, 33(4), 377–382. <http://www.ias.ac.in/matresci/bmsaug2010/377.pdf>
- Fukami, T., Hiyajyo, S., Tahara, S., & Yasuda, C. (2016a). Thermal properties, crystal structure, and phase transition of racemic $\text{CaC}_4\text{H}_4\text{O}_6 \cdot 4\text{H}_2\text{O}$ single crystals. *Am. Chem. Sci. J.*, 16(3), 28258 1–11. <http://dx.doi.org/10.9734/ACSJ/2016/28258>
- Fukami, T., Tahara, S., Yasuda, C., & Nakasone, K. (2016b). Structural refinements and thermal properties of L(+)-tartaric, D(–)-tartaric, and monohydrate racemic tartaric acid. *Inter. J. Chem.*, 8(2), 9–21. <http://dx.doi.org/10.5539/ijc.v8n2p9>
- Fukami, T., Tahara, S., Yasuda, C., & Nakasone, K. (2016c). Crystal structure and thermal properties of $\text{SrC}_4\text{H}_4\text{O}_6 \cdot 4\text{H}_2\text{O}$ single crystals. *Int. Res. J. Pure Appl. Chem.*, 11(1), 23674 1–10. <http://dx.doi.org/10.9734/IRJPAC/2016/23674>
- Gal, J. (2013). Citation for chemical breakthrough awards: Choosing pasteur's award-winning publication. *Bull. Hist. Chem.*, 38(1), 7–12. <http://www.scs.illinois.edu/~mainzv/HIST/awards/Citations/v38-1%20p7-12.pdf>

- Hawthorne, F. C., Borys, I., & Ferguson, R. B. (1982). Structure of calcium tartrate tetrahydrate. *Acta Crystallogr.*, *B38*(9), 2461–2463. <http://dx.doi.org/10.1107/S0567740882009042>
- Kader, M. M. A., El-Kabbany, F., Taha, S., Abosehly, A. M., Tahoon, K. K., & El-Sharkawy, A. A. (1991). Thermal and electrical properties of ammonium tartrate. *J. Phys. Chem. Solids*, *52*(5), 655–658. <http://www.sciencedirect.com/science/journal/00223697/52/5>
- Labutina, M. L., Marychev, M. O., Portnov, V. N., Somov, N. V., & Chuprunov, E. V. (2011). Second-order nonlinear susceptibilities of the crystals of some metal tartrates. *Crystallogr. Rep.*, *56*(1), 77–79. <http://dx.doi.org/10.1134/S1063774510061082>
- Lowry, T. M. (1923). Pasteur as chemist. *Proc. Roy. Soc. Med.*, *16*, 16–20. <http://www.ncbi.nlm.nih.gov/pmc/articles/PMC2104002/>
- Pasteur, M. L. (1848). Sur les relations qui peuvent exister la forme cristalline, la composition chimique et Le sens de la polarisation rotatoire. *Ann. Chim. Phys.*, *24*, 442–463. <http://gallica.bnf.fr/ark:/12148/bpt6k65691733/f446.image.r=Annales%20de%20chimie%20et%20de%20physique.langEN>
- Shah, A., & Patel, I. B. (2010). FTIR and XRD study of barium tartrate ($\text{BaC}_4\text{H}_4\text{O}_6$) crystals grown by gel method. *AIP conf. Proc.*, *1249*, 192–193. <http://dx.doi.org/10.1063/1.3466554>
- Sheldrick, G. M. (2015). Crystal structure refinement with SHELXL. *Acta Crystallogr.*, *C71*(1), 3–8. <http://dx.doi.org/10.1107/S2053229614024218>
- Silgo, C. G., Platas, J. G., Pérez, C. R., López, T., & Torres, M. (1999). Barium L-tartrate. *Acta Crystallogr.*, *C55*(5), 740–742. <http://dx.doi.org/10.1107/S0108270198016709>
- Song, Q. B., Teng, M. Y., Dong, Y., Ma, C. A., & Sun, J. (2006). (2S,3S)-2,3-Dihydroxy-succinic acid monohydrate. *Acta Crystallogr.*, *E62*(8), o3378–o3379. <http://dx.doi.org/10.1107/S1600536806021738>
- Torres, M. E., Peraza, J., Yanes, A. C., López, T., Stockel, J., López, D. M., ... & Silgo, C. G. (2002). Electrical conductivity of doped and undoped calcium tartrate. *J. Phys. Chem. Solids*, *63*(4), 695–698. <http://www.sciencedirect.com/science/journal/00223697/63/4>
- Weil, M. (2015). Crystal structure of lead(II) tartrate: a redetermination. *Acta Crystallogr.*, *E71*(1), 82–84. <http://dx.doi.org/10.1107/S2056989014027376>

Copyrights

Copyright for this article is retained by the author(s), with first publication rights granted to the journal.

This is an open-access article distributed under the terms and conditions of the Creative Commons Attribution license (<http://creativecommons.org/licenses/by/4.0/>).